Hindawi
International Journal of Polymer Science
Volume 2018, Article ID 2684962, 11 pages
https://doi.org/10.1155/2018/2684962

Research Article

Valorizing Rice Straw and Its Anaerobically Digested Residues for Biochar to Remove Pb(II) from Aqueous Solution

Jinyang Li,[1,2,3,4,5] Fei Shen,[1,2,3,4] Gang Yang,[3,4] Yanzong Zhang,[4] Shihuai Deng,[3,4] Jing Zhang,[3,4] Yongmei Zeng,[3,4] Tao Luo,[1,2] and Zili Mei[1,2]

[1]*Biogas Institute of Ministry of Agriculture, Chengdu 610041, China*
[2]*Key Laboratory of Development and Application of Rural Renewable Energy, Ministry of Agriculture, Chengdu 610041, China*
[3]*Institute of Ecological and Environmental Sciences, Sichuan Agricultural University, Chengdu, Sichuan 611130, China*
[4]*Rural Environment Protection Engineering & Technology Center of Sichuan Province, Sichuan Agricultural University, Chengdu, Sichuan 611130, China*
[5]*State Grid Sichuan Power Economic Research Institute, Chengdu, Sichuan 610041, China*

Correspondence should be addressed to Fei Shen; fishen@sicau.edu.cn

Received 2 November 2017; Accepted 1 February 2018; Published 20 March 2018

Academic Editor: Xuebing Zhao

Copyright © 2018 Jinyang Li et al. This is an open access article distributed under the Creative Commons Attribution License, which permits unrestricted use, distribution, and reproduction in any medium, provided the original work is properly cited.

To seek a new path to valorize rice straw (RS) and its anaerobically digested residues (DRS), biochar production at different temperatures for removing Pb(II) from aqueous solution and its basic physicochemical characteristics for elucidating potentially adsorption mechanisms were investigated. Overall, pH, electrical conductivity (EC), ash, specific surface area (SA), micronutrient content, and aromaticity of RS biochars (RSBCs) and DRS biochars (DRSBCs) increased with the promoted pyrolysis temperature, and opposite trends were found on the yield, volatile matter, H, N, and O. Lower pH and K content but higher yield, carbon stability, and N and P content were achieved by DRSBCs. Consequently, DRSBCs exhibited lower Pb(II) removal, which was 0.15–0.35 of RSBCs. Maximum adsorption capacities of 276.3 and 90.5 $mg \cdot g^{-1}$ were achieved by RSBC and DRSBC, respectively, at 500°C. However, distinct mechanisms dominated Pb(II) removal, in which carbonates and carboxylates were responsible for RSBCs, and phosphate silicate precipitation and complexation with carboxylate groups controlled DRSBCs.

1. Introduction

Rice is the staple food for over half the world's population. Approximately 480 million metric tons of milled rice is produced annually [1]. More than 90% rice are produced from Asian countries, in which China is the largest producer in the world; consequently, approximately 975 million metric tons of rice straw is generated annually in the fields [2]. It is reported that only 20% of rice straw produced in the world can be utilized, and the rest is left as waste [2, 3]. In most countries, the remaining rice straw is left undisturbed to serve as mulch, is ploughed into the ground as soil nutrients, or is directly disposed by open-burning in the fields, which leads to the serious air pollution and greenhouse gas emission in practice [4] and, thereby, is strictly prohibited in China. In addition, rice straw is also employed as part of the nutritional requirements of ruminant animals in most rice producing countries. However, low protein content, possession of phenolic properties, and high level of silica and lignin are negative to rice straw digestibility by ruminant animals [5]. Thus, seeking more paths for efficiently utilizing rice straw is meaningful to the sustainability of rice production. Recently, anaerobically digesting agricultural residues for biogas production, as an effective method, have been gradually popularized in all the world [6]. However, with the increased scale of anaerobic digestion, the disposal of digested residues has become an urgent issue to be solved.

At present, producing biochar, a carbon-containing material via pyrolyzing biomass in an oxygen-limited environment, has become one of the alternative ways to utilize the waste biomass, such as crop straw, forestry waste, and livestock manure [7, 8]. Its applications in sequestrating

carbon, remediating soil, improving soil quantity, and controlling pollutants make biochar more attractive and popularly investigated. Especially in pollutant control in water environment, many investigations indicate that the biochar can remove many types of organic and inorganic contaminants from the aqueous solutions [9]. Unlike most organic pollutants, inorganic pollutants, mainly heavy metals, are nonbiodegradable and may be transferred along the food chain via bioaccumulation [7]. Many studies have demonstrated that biochar has excellent performances to immobilize heavy metals in soil and water [10–12]. Thus, biochar is increasingly being considered as an alternative agent in water treatment technologies for removing heavy metals.

The mechanisms of removing heavy metals from aqueous solution by biochar are generally via precipitation, complexation, ion exchange, electrostatic interaction (chemisorption), and physical sorption [7]. The physical sorption is mainly depended on the surface areas and pore volumes. Although many biochars have been reported to have high surface area with well-distributed pore network, including micropores (<2 nm), mesopores (2–50 nm), and macropores (>50 nm) [13], it is well known that the pore development of biochar is not enough compared with the traditional activated char as biomass is carbonized directly for biochar without any activation processes [14]. Many biochars are reported as negatively charged surfaces, which can sorb positively charged metals through electrostatic attractions. However, prevalence of this mechanism in biochar-metal sorption process is dependent on the solution pH and point of zero charge (PZC) of biochar [13, 15]. Complexation (outer- and inner-sphere) involves the formation of multiatom structures (i.e., complexes) with specific metal-ligand interactions, which was mainly related to oxygen functional groups on the surface of biochar [16, 17]. Immobilizing heavy metals via ion exchange is another possible mechanism, which is closely related to the positively charged ions, such as Na, K, Ca, and Mg, on biochar surfaces and the cation exchange capacity (CEC) [18, 19]. By contrast, the precipitation has been widely accepted as one of the main mechanisms for removing heavy metals by biochar, which greatly related to the ash components of biomass, such as the elements of Ca, Mg, Fe, Cu, and Si [20, 21]. Obviously, the ash components in biomass may be potentially associated with the functions of ion exchange and precipitation and further affect the adsorption capacity to heavy metals. Rice straw, typically characterized by relatively higher ash content, thereby, can be potentially employed to immobilize heavy metals via precipitation or ion exchange. In addition, anaerobic digestion can convert part of organic matters, such as hemicellulose, cellulose, lignin, and other organic extractives into CH_4 and CO_2. Consequently, ash content of the anaerobically digested rice straw will be greatly promoted compared with the original rice straw. Considering the urgency for seeking the efficient paths of utilizing rice straw and its digested residues, their carbonization for producing biochar to remove heavy metals specially deserves being investigated in-depth.

Main sources of lead pollution in the environment are from lead-acid battery industry, mining, metal smelting, automobile exhaust, coal, and paint. At present, the main methods for treating lead pollution include chemical precipitation, redox, ion exchange, adsorption, reverse osmosis, and electrolysis. However, these technologies have some drawbacks, such as complex process, expensive chemical input, high running cost, inconvenient operation, and potential secondary pollution. In this context, the typical heavy metal ion of Pb(II) was selected as the model contaminant to investigate the adsorption performances of biochars derived from rice straw and its anaerobically digested residues. Meanwhile, different biochars from RS and DRS were obtained at an increasing pyrolytic temperature to seek their effects on Pb removal from aqueous solution. Correspondingly, the physical-chemical properties of biochars were discriminated by elemental analyses, scanning electron microscopy (SEM), Fourier transform infrared spectroscopy (FT-IR), and X-ray diffraction (XRD). The adsorption performances of biochars, concerning adsorption isotherm, kinetics, thermodynamics, and effects of solution pH were elaborated by batch experiments to discuss the possible adsorption mechanisms.

2. Materials and Methods

2.1. Rice Straw and Its Anaerobically Digested Residue. Rice straw (RS) was harvested from the local farm in Deyang, Sichuan province, and chopped in 2.0–3.0 cm for anaerobic digestion in a 100 L bioreactor. After 50 d batch digestion, the digested slurry was collected from outlet of the bioreactor. The solid residue of digested rice straw (DRS) was separated by filter, and it afterwards was air-dried for the following carbonization. Prior to pyrolysis, the RS and DRS were ground into powder (<0.45 mm, sieved) and dried at 105°C for 6.0 h to wipe off free moisture. The basic compositions of RS were analyzed for Klason insoluble lignin and carbohydrates as described in [22], and cellulose, hemicellulose, and lignin, were 14.0%, 30.8%, and 23.0%, and the corresponding compositions in DRS were 3.1%, 9.3%, and 44.4%, respectively.

2.2. Biochar Preparation. The dried RS and DRS were pyrolyzed in a tube furnace (OTL 1200, Nanjing Nanda Instrument Co., Ltd., China) under protective gas of N_2 (purity of 99.9%) with a flow rate of 0.1 $m^3 \cdot h^{-1}$. The heating rate of tube furnace was controlled at 10°C·min^{-1}, and the pyrolysis was maintained for 60 min after arriving at the designed temperature of 400°C, 500°C, 600°C, and 700°C. After pyrolysis, the furnace was cooled to room temperature for biochar collection. The derived biochar was weighted, and biochar yield was calculated according to the weights of biochar and the input RS and DRS. The obtained biochar from RS at different temperature was named as RS-400, RS-500, RS-600, and RS-700, respectively. The corresponding biochars from DRS were labeled as DRS-400, DRS-500, DRS-600, and DRS-700, respectively.

2.3. Characterization of Biochars. Proximate analysis, including ash, volatile matter, and fixed carbon, in RS, DRS, and their derived biochars, was performed according to the standard methods in the ASTM D 1762-84 [23]. The elemental compositions, including carbon, hydrogen, nitrogen, and oxygen, were determined using an elemental analyzer (EA112,

Thermo Finnigan, USA). pH and electric conductivity (EC) of biochars were measured by a pH meter (PHS-3C, LeiCi Instruments Co., Ltd., China) and a conductivity meter (DDS 12DW, BanTe Instruments Co., Ltd., China) with the ratio of 1 : 20 ($m \cdot v^{-1}$) for biochar to deionized water. The samples were digested in the concentrated HNO_3 and 30% H_2O_2 with the ratio of 3 : 1 for 24 h at 150°C to determinate the concentration of K, Na, Ca, Mg, and P. The elemental concentrations in the digested solution were determined by inductively coupled plasma spectroscopy (ICP-MS 7700s, Agilent, USA).

Thermal analysis of RS, DRS, and their corresponding biochars was conducted on a thermogravimetric analyzer (SDT Q600, TA instrument, USA) with the heating rate of 10°C·min^{-1} from 20°C to 700°C. The specific surface area (SA) of the biochars was measured by N_2 adsorption isotherms at 77 K (NOVA-2000E, Quantachrome Instruments, USA) with the Brunauer-Emmett-Teller (BET) method. The surface morphology of rice straw biochar (RSBC) and the digested rice straw biochar (DRSBC) were observed by a scanning electron microscopy (SU1510, Hitachi, Japan) to compare the apparent structure and surface characteristics. A Fourier transform infrared spectrometer (Nicolet 6700, Thermo Fisher Scientific, USA) was employed to identify the chemical functional groups of the original and Pb-loaded RSBC and DRSBC. The spectra were obtained by 64 scans of the sample in the range of 400–4000 cm^{-1} at a resolution of 4 cm^{-1}. In addition, the XRD analysis of RSBC, DRSBC, and Pb-loaded biochars were conducted on a computer-controlled diffractometer equipped with stepping motor and graphite crystal monochromator (I-2, Nicolet, Madison, WI, USA). The diffractometer was operated at 40 kV and 40 mA range from 5 to 70° with a scan speed of 1°·min^{-1}.

2.4. Adsorption. Pb(II) solution was prepared by dissolving analytic reagent grade $Pb(NO_3)_2$ in deionized water for batch adsorption with a concentration of 20–1200 mg·L^{-1} and 20 to 800 mg·L^{-1} for RSBC and DRSBC, respectively. 0.1000 g biochar was added to 150 mL screw-flasks filled with 50 mL Pb(II) solution and shaken at 120 r·min^{-1} for 24 h according to the kinetic result. After adsorption, the solutions were filtered through 0.45 μm filters and determined the residual Pb(II) concentration by an atomic adsorption spectrometer (FAAS-M6, Thermo, USA). As the thermodynamics were investigated, the batch adsorption was carried out at 15, 25, 35, and 45°C, respectively, with similar process. As the effects of pH were discussed, the Pb(II) solution was rapidly adjusted to the specified pH in equilibrium using 1.0 mol·L^{-1} HNO_3 or 1.0 mol·L^{-1} NaOH after 0.1 g biochar was added, and the batch adsorption was similar to the statement above. All runs for the adsorption were performed in triplicate, the presented data were the average of 3 reads.

3. Results and Discussion

3.1. Pyrolysis Behaviors and Biochar Yields of RS and DRS. Results of TG/DTG on RS and DRS are shown in Figure 1. The main mass loss stage of rice straw typically appeared in the range of 200–500°C with the maximum weigh loss at 340°C due to the decomposition of the typical fractions

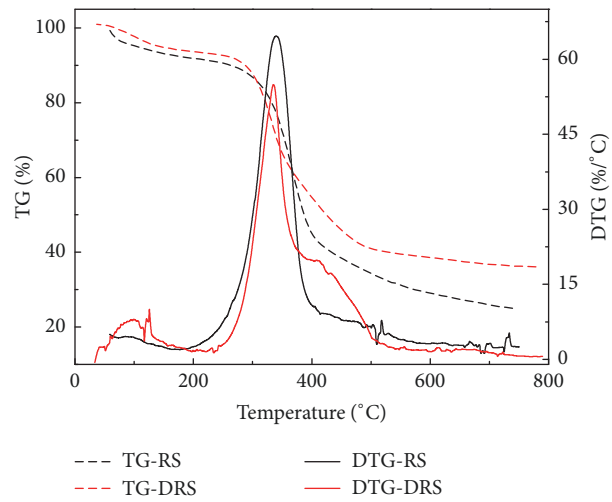

Figure 1: TG-DTG curves of RS and DRS.

of hemicellulose, cellulose, and lignin in the lignocellulosic biomass [24]. According to the DTG curve, the DRS was sharper than that of RS; however, the weight loss rate of DRS at 335°C was significantly lower than that of RS, indicating easier degradation via pyrolysis because most of hemicellulose and cellulose in the RS were degraded after anaerobic digestion, only 3.1% cellulose and 9.3% hemicellulose in DRS. An apparent peak at 408°C can be observed at DRS, because higher lignin remained to be undigested and the content of lignin increased from 23% to 44.4% after anaerobic digestion. Besides, the TG curves during final stage (400–750°C) indicated that more fix fraction will remain in DRS due to relatively higher ash content after anaerobic digestion. These results from TG/DTG basically responded to the composition change of RS after anaerobic digestion.

As shown in Table 1, the biochar yield decreased from 47.5% to 36.0% for the RS with the increase of pyrolysis temperature. By contrast, it was 74.9% to 57.5% for the DRS. The biochar yields of RS and DRS were both decreased rapidly from 400°C to 500°C but tended to be stable after 500°C. This was mainly because most organic matters were decomposed rapidly and only a few lignin dissociated in the pyrolysis process when the pyrolysis temperature over 500°C. Overall, the biochar yield from DRS was promoted by 21.5–27.4% compared with RS due to the relatively higher ash content in DRS, which was basically consistent with the results from TG/DTG.

3.2. Characterization of Biochar

3.2.1. Thermal Stability. Weight loss peaks appeared at 100°C in all biochars, mainly due to the dehydration of free water and bound water (see Figure S1). In contrast to the corresponding raw materials of RS and DRS, there was no obvious mass loss within 200–400°C because of the decomposition of hemicellulose, cellulose, and lignin during the pyrolysis process [25]. As RSBC was obtained at lower temperature of 400°C, 3 obvious weight loss peaks were detected at 335, 425, and 465°C, respectively, which was mainly due to the residual

Table 1: Physicochemical properties of biochars produced at different temperatures.

	Yield %	Ash %	FC[b] %	VM[c] %	EC (ms)	pH	SA ($m^2 \cdot g^{-1}$)	K ($g \cdot kg^{-1}$)	Na ($g \cdot kg^{-1}$)	Ca ($g \cdot kg^{-1}$)	Mg ($g \cdot kg^{-1}$)	P ($g \cdot kg^{-1}$)
RS	N.A.[a]	15.43	7.57	68.58	N.A.	N.A.	N.A.	17.60	0.28	8.34	1.81	0.88
RS-400	47.45	31.87	21.88	38.05	4.70	9.81	270.84	28.31	0.49	11.70	4.31	2.50
RS-500	39.25	35.01	33.30	24.73	5.32	10.89	314.86	38.80	0.69	11.37	5.82	3.22
RS-600	36.35	41.09	33.33	19.16	5.73	11.1	465.21	40.39	0.61	40.51	5.39	3.29
RS-700	36.00	42.16	34.65	17.20	5.77	11.18	404.97	40.69	0.71	11.33	4.90	3.06
DRS	N.A.	43.77	4.48	46.78	N.A.	N.A.	N.A.	5.01	1.21	40.47	5.54	13.74
DRS-400	74.85	57.36	8.07	31.13	0.57	8.6	117.42	6.75	1.62	51.82	7.34	20.19
DRS-500	63.16	64.18	13.95	18.04	0.74	9.12	137.50	6.50	1.57	52.07	7.66	21.03
DRS-600	59.70	69.01	12.46	14.97	0.69	9.52	162.00	8.62	2.04	256.91	9.61	25.38
DRS-700	57.52	70.82	14.76	11.04	0.79	9.73	213.27	8.60	2.12	174.85	8.96	25.61

Note. [a]N.A. means not applicable; [b]FC is fixed carbon; [c]VM is volatile matter.

cellulose and lignin after carbonization. Nevertheless, only one peak of lignin loss appeared at 470°C in DRS-400. A peak of weight loss still could be detected in DRS-500, but RS-500 peak could not be observed in the same area, which again implied the rich-lignin in DRS. With increasing pyrolysis temperature, the weight loss of RSBCs and DRSBCs were weakened within 400–550°C, which due to the carbonization was not complete during carbonization at middle temperature (400 and 500°C), and the residual cellulose and lignin were further pyrolyzed and released as volatile matters. By contrast, the biochars prepared at high temperatures (600 and 700°C) were relatively complete, suggesting relatively higher thermal stability. All biochars had a weak weight loss peak after 650°C, which was mainly due to the decomposition of mineral substances in the ash, for example, $CaCO_3 \rightarrow CaO$ [26]. Overall, DRSBCs have less mass loss compared with RSBCs being obtained at the investigated temperatures, implying relatively higher thermal stability.

3.2.2. Proximate Analysis on the Derived Biochars. As is known, fixed carbon (FC) and volatile matter (VM) can evaluate the biochar stability against the biological degradation [27]. Pyrolysis temperature exhibited a positive correlation with the FC content but negatively affected VM content in the biochar from both of RS and DRS, which were also observed in reference [28]. Overall, FC content decreased 13.8–20.9% in DRSBCs compared with the corresponding RSBCs at the investigated pyrolytic temperatures. Similarly, VM content in DRSBCs was reduced 4.2–6.9%. Ash content enhanced obviously as the pyrolysis temperature was increased, indicating more organic components in the RS and DRS were pyrolyzed at high temperature. Moreover, the ash in DRSBCs was 25.5–29.2% higher in contrast to the corresponding RSBCs, which was consistent to the biochar yield, suggesting biochar yields of RS and DRS were ash-dependent. High amounts of mineral elements, especially higher content of silicon, in rice straw, will lead to high ash content of the derived biochar (RSBCs) [29]. Relatively higher ash content in DRSBCs again indicated the organic fractions was decomposed and retained indigestibility mineral composition during anaerobic digestion process.

3.2.3. Ultimate Analysis. As expected, the elemental contents of H and O were reduced with increasing pyrolysis temperature (see Table S1). The C content in RSBCs was increased from 41.1% to 44.1% as the temperature was elevated from 400°C to 600°C, which was consistent with the biochar produced form traditional lignocellulosic biomass [8]. However, a slight decrease (43.8%) was observed at 700°C. Unlike the traditional lignocellulosic biomass with relatively lower ash content, the C content in DRSBCs exhibited obvious decrease with the increase of pyrolysis temperature. According to many reported works, it could be found that the biomass with lower ash content, and the increased C content with increasing pyrolytic temperature could be observed; however, the contrary results on C content will appear in the higher ash content biomass, such as swine manure, vermicompost, and sludge [19, 30, 31]. Obviously, the mineral fractions in ash-abundant biomass will function as the heat transmitter to intensify the release of volatile matters during pyrolysis [32]. Moreover, the relatively lower organic fraction (most of them were decomposed by biological process) in such substrates will more easily be pyrolyzed into low molecular weight compounds for rapid releasing. The decreased H/C and O/C ratios at higher pyrolysis temperature indicated more stability of RSBC and DRSBC [8]. As for the N content in biochars from RS and DRS, obvious decreases with increasing pyrolysis temperature can be observed, which was due to the volatilization in the form of NOx and NH_3 during the generation of waste gases [33]. However, significant increases also could be observed as the pyrolysis temperature kept increasing to 700°C, which was mainly related to the formation of stable N-derivatives or N-doping into complex structures at relatively higher temperatures [28, 34]. Relatively higher C content in DRSBCs suggested the stable N formation at higher temperature would be related to the ash content. However, the detailed production of stable N still required more investigations.

Besides, the contents of Na, Ca, Mg, and P in RS were all obviously lower than that of DRS. Correspondingly, their contents in the obtained biochars from RS were all lower than that of DRS. However, K content in RS was significantly higher than that of DRS, resulting in its relatively lower

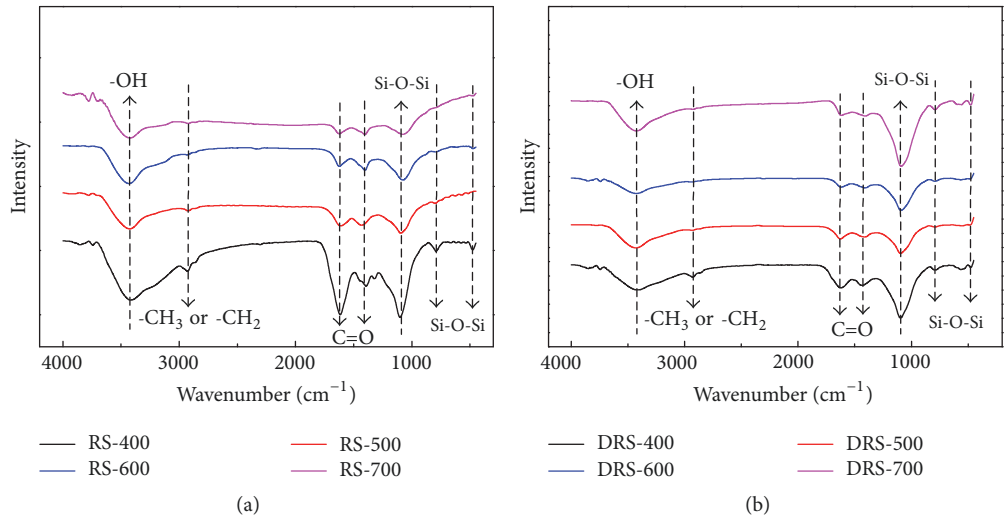

Figure 2: FT-IR spectra for RSBCs and DRSBCs. (a) RSBC; (b) DRSBC.

content in RSBCs correspondingly. These results indicated K in rice straw will be released more in the liquid fraction after anaerobic digestion, and the other investigated elements above will be kept more in the digested solid residue. K as a critical element for catalyzing the melting of silica in rice pyrolysis may affect the crystalline properties of the silicate particles and further the function of the produced biochars [35]. Overall, the content of K, Na, Ca, and Mg in biochar increased with the rising of temperature, indicating that the prepared biochars at high temperature can exhibit ion exchange capacity and can be potentially beneficial to the adsorption of heavy metals via ion exchange. However, the Ca and Mg content in both of RSBCs and DRSBCs reduced significantly at extra higher temperature of 700°C due to the volatilization via pyrolytic gas, and this result was consistent with the previous report on another kind of digested residue of vermicompost [19].

3.2.4. pH, EC, and Functional Groups. As expected, the investigated biochar is alkaline due to the abundance of alkali and alkaline earth metals. Moreover, the increased pH with increasing the pyrolysis temperature could be observed on RSBCs and DRSBCs as the mineral substances, especially the alkaline earth metals, could be decomposed into the corresponding oxides. The pH of DRSBCs was lower than that of RSBCs, which may relate to the relatively lower content of a main alkali metal of K in DRSBCs. In addition, some acid substances like humic acid, which produced in anaerobic fermentation, may also contribute to relatively lower pH in DRSBCs [36]. Overall, the EC enhanced with the increase of temperature, which was positively correlated with the soluble salt content in biochar. Overall, the SA of RSBCs and DRSBCs was increased with the increase of temperature, but a reduction appeared at high temperature (700°C) of RSBC, which was due to the rearrangement of the chemical structure and part of the pore size collapsed at high temperatures [37]. Furthermore, the RSBC produced at different temperatures exhibited typical higher SA compared with that of DRSBC, which may be attributed to the richer lignocellulosic faction in RS, and similar results were also reported in [38]. The scanning electron microscopy images (Figure S2) showed that RSBC had more multiple voids and micropores because of the dehydration of lignocellulose [29]. Conversely, the DRSBC images showed more crystalline and less porous structure, implying a relatively lower lignocellulosic fraction content.

According to the FT-IR spectra of RSBCs and DRSBCs in Figure 2, the band intensities at 3400–3430 cm^{-1} (-OH) and 2850–2950 cm^{-1} (aliphatic CH_2) decreased when the pyrolysis temperature was increased because of the thermal destruction of cellulose, hydroxyl groups, and aliphatic alkyl groups. Similarly, the features (C=O) between 1630 and 1580 cm^{-1} and between 1430 and 1390 cm^{-1} were decreased due to the thermal destruction of aliphatic matter and hydroxyl groups. The aromatic carbon remained after pyrolysis in high temperatures which is more inert than aliphatic carbon under oxidation conditions [39]. Therefore, the high-temperature derived biochars are more recalcitrant and may have lower adsorption capacity. The intensity of carboxylate groups (C=O stretching) are stronger in RSBCs, which can serve as adsorption sites for metals [40]. Thus, RSBCs may have better heavy metal adsorption ability than DRSBCs. 3 features at 1100, 800, and 470 cm^{-1} are assigned to the vibration of Si-O-Si. Si group in RSBCs became less intense with increasing pyrolytic temperature, implying the formation of silicon crystal at high temperature [40]. All biochars exhibit a strong Si-O-Si stretching band, which means RSBCs and DRSBCs could act as a novel silicon source due to its high silicon content [39].

3.3. Pb(II) Adsorption via the Derived Biochars from RS and DRS as Affected by Pyrolysis Temperature. Overall, the considerable Pb(II) removal from aqueous solution could be achieved by RSBCs. According to Figure 3, the adsorption of Pb(II) was promoted significantly as the pyrolysis

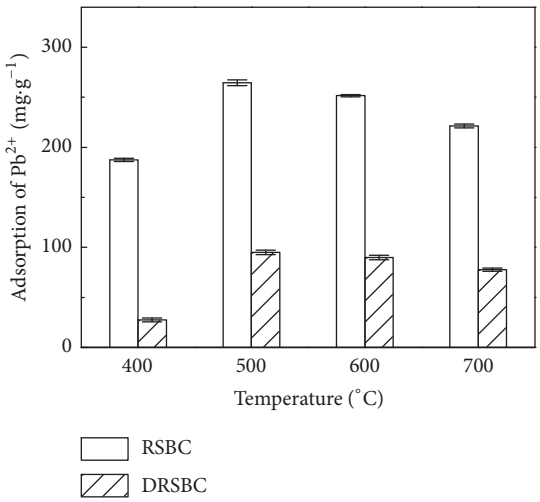

Figure 3: Pb(II) adsorption of biochars obtained at different pyrolysis temperatures.

temperature for producing biochar increased from 400°C to 500°C. The maximum adsorption capacity of 264.4 $mg \cdot g^{-1}$ appeared at RSBCs obtained from 500°C. Afterwards, the adsorption was reduced obviously to 221.3 $mg \cdot g^{-1}$ when pyrolysis temperature was increased to 700°C. Similar effects of pyrolysis temperature on the Pb(II) adsorption also happened on the biochar from DRS. Previous studies have shown the same result that biochar adsorption capacity improved as the pyrolytic temperature from 300°C to 500°C but did not increase when the pyrolysis temperature was kept increasing to 600°C [28]. In addition, the increased Pb(II) adsorption may be related to the increased SA as the pyrolysis temperature was lower than 500°C. Besides, the decreased Pb(II) adsorption was observed as the pyrolysis was higher than 500°C, indicating it may be affected negatively by another action. Previous studies have proved that the adsorption of heavy metals on biochar may be also mainly related to the interaction between surface functional groups and minerals [26]. The decreased oxygen functional groups on these biochars at higher pyrolysis temperature may partially decrease the Pb(II) adsorption (Figure 2). In addition, the Ca, Mg, P, and inorganic elements formed insoluble phosphate and carbonate crystals in high-temperature biochar which could slow the release rate of PO_4^{3-} and CO_3^{2-}, thereby reducing the reaction with Pb(II) via precipitation [41]. Based on these results, the adsorption of Pb(II) by RSBC and DRSBC may be related to the coactions of the development of SA, oxygen functional groups, and the anions involved in precipitation. Apparently, the Pb(II) removal from aqueous solution by DRSBCs was 0.15–0.35 of RSBCs, which may greatly be attributed to the loss of some surface functional groups and soluble salts during anaerobic digestion and the decreased SA as well [42].

3.4. Pb(II) Adsorption Behaviors of RSBC and DRSBC. According to the effects of pyrolysis temperature on Pb(II) adsorption, the biochar produced at 500°C from RS and DRS was selected to elucidate the adsorption behaviors via investigating the isotherms, kinetics, and thermodynamics. As presented in Figure S3a, the adsorption capacity of RSBC and DRSBC was elevated with the increase of initial Pb(II) concentration. The Pb(II) adsorption capacity of RS-500 and DRS-500 rapidly enhanced as the initial concentration of Pb(II) was lower than 500 $mg \cdot L^{-1}$ and 200 $mg \cdot L^{-1}$, respectively. Correspondingly, the Pb(II) could be almost removed completely at these concentrations. However, the adsorption tended to be balanced as Pb(II) initial concentrations kept increasing. This phenomenon was generally depended on the fact that the competitive adsorption for Pb(II) on RSBC and DRSBC surface sites was not obvious at the relatively lower concentrations, while their fiercely competition emerged as the Pb(II) concentration increased greatly. Langmuir (Eq. S1) and Freundlich (Eq. S2) isotherms have been widely accepted to describe the relationship between the concentration of adsorbate on adsorbent surface and in solution at equilibrium. In contrast to the Freundlich model (Figure 4(a) and Table S2), the higher correlation coefficient can be obtained by Langmuir model ($R^2 > 0.83$), demonstrating that the adsorptions of Pb(II) by RS-500 and DRS-500 were both based on monolayer homogeneous adsorption process. The maximum Pb(II) adsorption capacity of RS-500 and DRS-500 was determined as 276.3 and 90.5 $mg \cdot g^{-1}$, respectively, which was typically higher than most of the low cost adsorbents, such as anaerobically digested animal waste biochar (51.4 $mg \cdot g^{-1}$) and sludge biochar (30.9 $mg \cdot g^{-1}$) [43, 44]. This result implied that RSBC and DRSBC exhibited an excellent adsorption ability to remove Pb(II) from aqueous solution. Notably, the removal rate of RS-500 was very low as the initial Pb(II) concentration was less than 100 $mg \cdot L^{-1}$; however, almost no Pb(II) was detected in DRS-500 equilibrium solution even at initial Pb(II) concentration of 20 $mg \cdot L^{-1}$. Therefore, DRSBC should be more suitable for removing Pb(II) at low concentration compared with that of RSBC. The affinities between Pb(II) and biochar can be further predicted by using dimensionless separation factor R_L (Eq. S3). $1 > R_L > 0$, $R_L = 1$ and $R_L > 1$ indicate that the shape of isotherm is favorable, linear, and unfavorable, respectively. According to the RS-500 and DRS-500 parameters of Langmuir, the calculated R_L was 0.56 and 0.046, respectively, suggesting that the adsorption of Pb(II) on RS-500 and DRS-500 was favored.

Pb(II) adsorption of RS-500 was rapidly performed during the initial 2 h, and the removal of Pb(II) exceeded 215 $mg \cdot L^{-1}$ (Figure S3b). However, the adsorption gradually slowed down and reached equilibrium at 12 h. This could be regarded as large amount of vacant adsorption sites on the surface of RSBC were offered at initial stage, and the surface sites were progressive saturation and almost occupied as time was prolonged [43, 44]. Pb(II) adsorption of DRS-500 did not reach adsorption equilibrium in 48 hours, because DRS-500 is a relatively dense massive accumulation structure (Figure S2), which may lead to the adsorption sites be covered, resulting in slower reaction with Pb(II). Additionally, Pb(II) can be adsorbed by the precipitation of the anions released from biochar, and the reaction rate depends on the dissolution rate of the mineral components. Most of the minerals in RSBC are

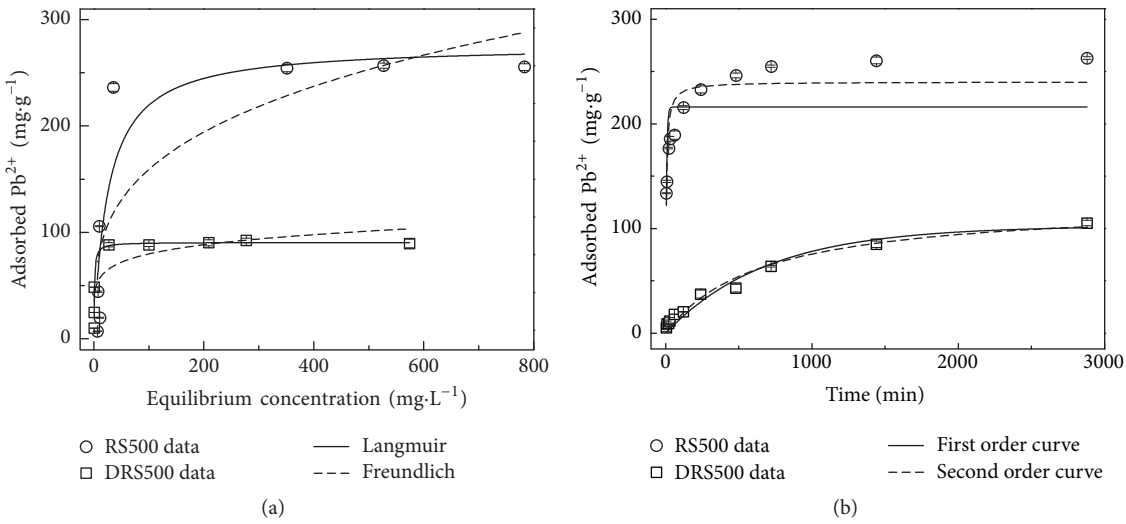

Figure 4: Adsorption isotherms and kinetics of Pb(II) adsorption on biochars: (a) adsorption isotherms of RS-500 and DRS-500; (b) adsorption kinetics of RS-500 and DRS-500.

amorphous and easily soluble mineral salts, which can release anions more easily and faster to precipitate with Pb(II) [41]. However, DRSBC formed more crystalline minerals, which was more difficult to dissolve. Even though a small amount of crystalline minerals can be dissolved, the dissolution rate is relatively slow; thereby the biochar adsorption of Pb(II) became slow. The kinetics of Pb(II) adsorption on RS-500 and DRS-500 were described by first-order (Eq. S4) and second-order (Eq. S5) model (Figure 4(b)), respectively. It can be known that the second-order model gives better simulation on both RS-500 and DRS-500 (Table S3), further confirming that the adsorption rate is greatly governed by chemisorption mechanism [45]. The second-order model (R^2 = 0.96) appeared to better describe adsorption of DRS-500 rather than RS-500 (R^2 = 0.87), partially suggesting that precipitation and inner-sphere surface complexation could also play an important role in Pb(II) adsorption by RS-500.

The Gibbs free energy (ΔG^0), enthalpy (ΔH^0), and entropy (ΔS^0) are generally considered to be important parameters to understand adsorption mechanisms. The equations were exhibited in Eq. S6–Eq. S8 and calculated results were given in Table S4. The values of ΔG^0 were negative to the adsorption temperatures, indicating that the adsorption process is spontaneous. The elevated ΔG^0 with the increasing temperature illustrated that the adsorption process of RS-500 and DRS-500 can be favored by temperature, which can be again proved in Figure S3d. As the temperature was elevated from 15 to 45°C, the Pb(II) adsorption capacity of RS-500 and DRS-500 can be increased from 245.1 $mg \cdot g^{-1}$ to 254.5 $mg \cdot g^{-1}$ and 63.0 $mg \cdot g^{-1}$ to 140.8 $mg \cdot g^{-1}$, respectively. This phenomenon could be attributed to the promoted occasion of collision between adsorption sites and Pb(II) ions at higher adsorption temperature [12]. The ΔH^0 values of RS-500 and DRS-500 were 0.244 $KJ \cdot mol^{-1}$ and 4.038 $KJ \cdot mol^{-1}$, suggesting the adsorption process was endothermic and the random thermal motion of ions in the aqueous solution has significant effects on Pb(II) adsorption of DRSBCs. The values of ΔS^0 were 5.9 and 18.0 $J \cdot mol^{-1} \cdot K^{-1}$, elucidating that RS-500, DRS-500, and Pb(II) were closely combined. In addition, increasing the adsorption temperature can increase the degree of freedom between adsorbate and adsorbed on solid-liquid interface [46]. DRS-500 had high activation entropy values, meaning that DRS-500 is far from its own thermodynamic equilibrium and the system can react faster to produce the activated complex [47]. Thus, complexation may play a more important role in DRSBCs than RSBCs.

Besides, as presented in Figure S3c, the adsorption of Pb(II) by RS-500 was enhanced by pH of solution, indicating that the lower pH resulted in the larger competition interaction between H^+ and Pb(II). Diversely, when the pH increased from 2.0 to 4.0, the DRS-500 adsorption capacity of Pb(II) was decreased from 115.1 $mg \cdot g^{-1}$ to 92.6 $mg \cdot g^{-1}$. In addition, SiO_2 is negatively charged at low pH (pH < 3.0) because its lower isoelectric point and the solution pH also can influence silicon dissolution from biochar [39, 48]. Therefore, the increase of DRS500 adsorption capacity at low pH value is mainly attributed to the contribution of SiO_2 components.

3.5. Potential Mechanisms for Pb(II) Adsorption by RSBC and DRSBC. As stated above, Pb(II) adsorption by RSBC and DRSBC was both decreased slightly as the SA was promoted greatly with the increased pyrolysis temperature. This result suggested the adsorption related to the increased surface area was not dominant. According to the FT-IR results on RSBC and DRSBC before/after Pb(II) adsorption (Figure S4), some bands shift after adsorption indicated the existing interactions between Pb(II) and the functional groups. For example, the shift of the COO- symmetric stretching to lower frequency (1433 → 1405 and 1420 → 1407 cm^{-1}) could be due to the low electron density induced by Pb(II) adsorption on RS-500 and DRS-500, respectively [49]. A

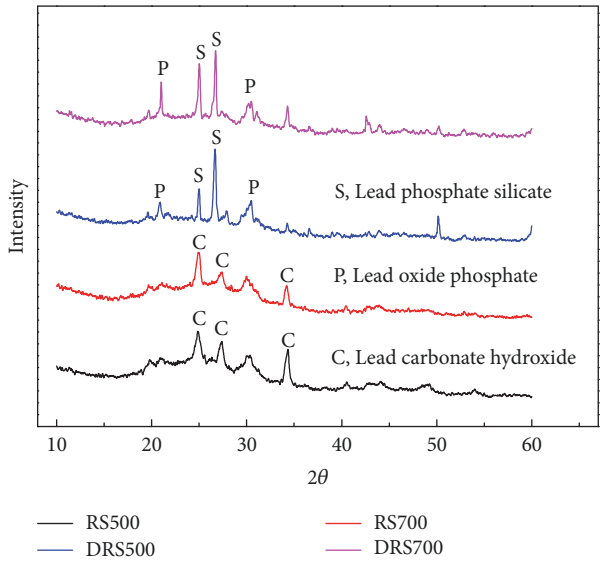

Figure 5: XRD diffraction patterns for RSBC-Pb and DRSBC-Pb.

shift of the COO- asymmetric stretching band to higher frequency (1611 → 1615 and 1622 → 1625 cm^{-1}) was also observed after Pb(II) adsorption on RS-500 and DRS-500, which likely resulted from the protonation of the carboxylate groups [49]. Thus, one possibility for Pb(II) adsorption by biochar from RS and DRS can be described as follows, revealing surface complexation via coordination between the carboxylate groups and Pb(II) is an important path (Eq. (1)).

$$\text{>C-COOH} + Pb^{2+} + H_2O \longrightarrow \text{>C-COOPb}^{+} + H_3O^{+} \quad (1)$$

In addition, the bands at 470, 800, and 1100 cm^{-1} were characteristic of Si-O-Si bend stretching, symmetric stretching, and asymmetric stretching, respectively [50]. After Pb(II) adsorption, these peaks were shifted and became less intense, which indicated that Pb(II) may relate to the existing structure of Si-O-Si; however, the substantial process deserved further investigations.

To further elucidate the interaction between minerals and Pb(II), XRD analysis was also conducted after Pb(II) adsorption as shown in Figure 5. Elemental analysis shows that DRSBC was rich in P, which was much higher than RSBC (Table 1). Previous research has shown that introducing P in biochar induced formation of insoluble lead phosphate minerals in Pb-polluted water [51]. XRD showed the precipitation of crystalline β-$Pb_9(PO_4)_6$ formation in DRS-500 after Pb(II) adsorption. Similarly, β-$Pb_9(PO_4)_6$ was also found in previous study on Pb(II) sorption on biochar converted from dairy manure [52]. The potential action process of the released phosphate from DRSBC with Pb(II) in aqueous solution can be deduced as the following equation to form stable minerals:

$$6HPO_4^{2-} + 9Pb^{2+} + 6OH^{-} \longrightarrow Pb_9(PO_4)_6 + 6H_2O \quad (2)$$

Besides, a sharp peak of $PbO{\cdot}P_2O_5{\cdot}SiO_2$ (lead phosphate silicate), with the typical 26.68 in the 2θ degree, was observed in Figure 5. The lead phosphate silicate precipitation was also reported by previous study [53]. The formation of lead phosphate silicate may be attributed to the reactions with lead and crystalline silica and phosphate on DRSBC, which may be the following reaction:

$$2HPO_4^{2-} + Pb^{2+} + SiO_2 \longrightarrow PbO{\cdot}P_2O_5{\cdot}SiO_2 + 2OH^{-} \quad (3)$$

However, only one lead precipitate $Pb_3(CO_3)_2(OH)_2$ (hydrocerussite) was found on the postsorption RSBC. We hypothesized that higher lead removal by RSBC may be attributed to formation of Pb-carbonate precipitate, which was confirmed by three hydrocerussite peaks in XRD. Contrary to DRSBC, higher pH (Table 1) and carbonate concentrations allowed for precipitation of hydrocerussite, which can be described as follows:

$$2HCO_3^{-} + 3Pb^{2+} + 4OH^{-} \longrightarrow Pb_3(CO_3)_2(OH)_2 + 2H_2O \quad (4)$$

Silica is also a major mineral component in rice straw [53], but there was no Pb-Si precipitation found on the postsorption RSBC. Based on these results, the interactions of Si-rich minerals with Pb(II) probably depend on Si crystallinity and the distinct crystalline substances in DRSBC, which may result from the elimination of K element [40]. Because K is a critical element to catalyze the melting of silica [35], the silicate particles in RSBC were more amorphous than DRSBC, which was potentially supported by the observations from SEM and XRD. In addition, the inferior removal rate of RS-500 at lower initial Pb(II) concentration (Figure S3a) is probably because solution calcium and magnesium remained unchanged till Pb > 0.5 mM [52]. Increased Ca^{2+} and Mg^{2+} are attributed to the dissolution of some Mg-substituted calcite [26], which also can provide more carbonate for hydrocerussite precipitation.

4. Conclusions

Biochars obtained from anaerobically digested rice straw (DRSBCs) showed lower pH value and potassium content, but higher yield, nitrogen, phosphorous content, and carbon stability compared with the biochars derived from rice straw (RSBCs). The biochars obtained at 500°C from both DRS and RS exhibited the highest performance for removing Pb(II) from aqueous solution. However, Pb(II) removal by RSBCs was typically higher than those of DRSBCs by 2.8–6.5-folds. As biochars produced at 500°C were selected, the maximum adsorption capacity of RSBC and DRSBC to Pb(II) arrived at 276.3 and 90.5 $mg{\cdot}g^{-1}$, respectively, according to the Langmuir model. Carbonates and carboxylates were contributed for the relatively higher adsorption capacity of RSBC. Pb(II) adsorption of DRSBC was dominated via forming phosphate silicates precipitation and complexing with carboxylate groups.

Conflicts of Interest

The authors declare that they have no conflicts of interest in this work.

Acknowledgments

This work is supported by the National Science & Technology Pillar Program (2015BAD21B03), the Special Fund for Agro-Scientific Research in the Public Interest (201403019), and the Agricultural Science and Technology Innovation Program (ASTIP) of Chinese Academy of Agricultural Sciences. Department of Science and Technology of Sichuan Province is also appreciated for funding supports (nos. 2017HH0047, 17ZDYF2972, and 2015NZ0100).

Supplementary Materials

(1) Supplementary Equation List: Supplementary Eq. 1: Langmuir model for Pb adsorption isotherm; Supplementary Eq. 2: Freundlich model for Pb adsorption isotherm; Supplementary Eq. 3: separation factor based on Langmuir model; Supplementary Eq. 4: the first-order model for Pb adsorption kinetics; Supplementary Eq. 5: the second-order model for Pb adsorption kinetics; Supplementary Eq. 6: model for Gibbs free energy; Supplementary Eq. 7: calculation for partition coefficient; Supplementary Eq. 8: linearized model for Gibbs free energy. (2) Supplementary Figures: Supplementary Figure 1: TG-DTG curves of biochars obtained at different temperatures; Supplementary Figure 2: the images of RSBCs and DRSBCs under the scope of SEM; Supplementary Figure 3: influences of reaction conditions, including initial concentration, temperature, duration, and pH, on Pb adsorption by RS-500 and DRS-500; Supplementary Figure 4: FT-IR spectra of the biochars of RS500 and DRS500 (after Pb adsorption). (2) Supplementary Tables: Supplementary Table 1: the results of elemental analysis of biochars produced at different temperatures; Supplementary Table 2: the calculated isotherm parameters of Pb adsorption on the biochars of RS-500 and DRS-500; Supplementary Table 3: the calculated kinetic parameters of Pb adsorption on the biochars of RS-500 and DRS-500; Supplementary Table 4: the calculated thermodynamic parameters of Pb adsorption on the biochars of RS-500 and DRS-500. *(Supplementary Materials)*

References

[1] S. Muthayya, J. D. Sugimoto, S. Montgomery, and G. F. Maberly, "An overview of global rice production, supply, trade, and consumption," *Annals of the New York Academy of Sciences*, vol. 1324, no. 1, pp. 7–14, 2014.

[2] R. Singh, M. Srivastava, and A. Shukla, "Environmental sustainability of bioethanol production from rice straw in India: A review," *Renewable & Sustainable Energy Reviews*, vol. 54, pp. 202–216, 2016.

[3] E. M. Hanafi, H. H. El Khadrawy, W. M. Ahmed, and M. M. Zaabal, "Some observations on rice straw with emphasis on updates of its management," *World Applied Sciences Journal*, vol. 16, no. 3, pp. 354–361, 2012.

[4] Y. Miura, T. Kanno, and Y. Miura, "Emissions of trace gases (co2, co, ch4, and n2o) resulting from rice straw burning," *Soil Science & Plant Nutrition*, vol. 43, no. 4, pp. 849–854, 1997.

[5] Y. Oladosu, M. Y. Rafii, N. Abdullah et al., "Fermentation quality and additives: a case of rice straw silage," *BioMed Research International*, vol. 2016, Article ID 7985167, 2016.

[6] C. M. Liu, A. C. Wachemo, H. R. Yuan et al., "Evaluation of methane yield using acidogenic effluent of NaOH pretreated corn stover in anaerobic digestion," *Journal of Renewable Energy*, vol. 116, pp. 224–233, 2017.

[7] M. I. Inyang, B. Gao, Y. Yao et al., "A review of biochar as a low-cost adsorbent for aqueous heavy metal removal," *Critical Reviews in Environmental Science and Technology*, vol. 46, no. 4, pp. 406–433, 2016.

[8] L. Ye, J. Zhang, J. Zhao, Z. Luo, S. Tu, and Y. Yin, "Properties of biochar obtained from pyrolysis of bamboo shoot shell," *Journal of Analytical and Applied Pyrolysis*, vol. 114, pp. 172–178, 2015.

[9] D. Mohan, A. Sarswat, Y. S. Ok, and C. U. Pittman, "Organic and inorganic contaminants removal from water with biochar, a renewable, low cost and sustainable adsorbent—a critical review," *Bioresource Technology*, vol. 160, pp. 191–202, 2014.

[10] Q. Cheng, Q. Huang, S. Khan et al., "Adsorption of Cd by peanut husks and peanut husk biochar from aqueous solutions," *Ecological Engineering*, vol. 87, pp. 240–245, 2016.

[11] J. H. Park, Y. S. Ok, S. H. Kim et al., "Competitive adsorption of heavy metals onto sesame straw biochar in aqueous solutions," *Chemosphere*, vol. 142, pp. 77–83, 2016.

[12] Z. Wang, F. Shen, D. Shen, Y. Jiang, and R. Xiao, "Immobilization of Cu2 + and Cd2 + by earthworm manure derived biochar in acidic circumstance," *Journal of Environmental Sciences*, vol. 53, pp. 293–300, 2017.

[13] A. Mukherjee, A. R. Zimmerman, and W. Harris, "Surface chemistry variations among a series of laboratory-produced biochars," *Geoderma*, vol. 163, no. 3-4, pp. 247–255, 2011.

[14] C. Kirbiyik, A. E. Putun, and E. Putun, "Comparative studies on adsorptive removal of heavy metal ions by biosorbent, biochar and activated carbon obtained from low cost agro-residue," *Water Science and Technology*, vol. 73, no. 2, pp. 423–436, 2016.

[15] X. L. Dong, L. Q. Ma, and Y. C. Li, "Characteristics and mechanisms of hexavalent chromium removal by biochar from sugar beet tailing," *Journal of Hazardous Materials*, vol. 190, no. 1–3, pp. 909–915, 2011.

[16] Z. Liu and F. Zhang, "Removal of lead from water using biochars prepared from hydrothermal liquefaction of biomass," *Journal of Hazardous Materials*, vol. 167, no. 1–3, pp. 933–939, 2009.

[17] D. Mohan, C. U. Pittman Jr., M. Bricka et al., "Sorption of arsenic, cadmium, and lead by chars produced from fast pyrolysis of wood and bark during bio-oil production," *Journal of Colloid and Interface Science*, vol. 310, no. 1, pp. 57–73, 2007.

[18] O. R. Harvey, B. E. Herbert, R. D. Rhue, and L. Kuo, "Metal interactions at the biochar-water interface: Energetics and structure-sorption relationships elucidated by flow adsorption microcalorimetry," *Environmental Science & Technology*, vol. 45, no. 13, pp. 5550–5556, 2011.

[19] G. Yang, Z. Wang, Q. Xian et al., "Effects of pyrolysis temperature on the physicochemical properties of biochar derived from vermicompost and its potential use as an environmental amendment," *RSC Advances*, vol. 5, no. 50, pp. 40117–40125, 2015.

[20] S. H. Ho, Y. D. Chen, Z. K. Yang, D. Nagarajan, J. S. Chang, and N. Q. Ren, "High-efficiency removal of lead from wastewater by

biochar derived from anaerobic digestion sludge," *Bioresource Technology*, 2017.

[21] D. Zhou, S. Ghosh, D. Zhang et al., "Role of Ash Content in Biochar for Copper Immobilization," *Environmental Engineering Science*, vol. 33, no. 12, pp. 962–969, 2016.

[22] R. Bura, S. D. Mansfield, J. N. Saddler, and R. J. Bothast, "SO2-catalyzed steam explosion of corn fiber for ethanol production," *Applied Biochemistry and Biotechnology - Part A Enzyme Engineering and Biotechnology*, vol. 98-100, pp. 59–72, 2002.

[23] C. M. Elsik, B. Devisetty, and S. W. Dean, "Round-Robin Evaluation of ASTM Standard Test Method E2798 for Spray Drift Reduction Adjuvants," *Journal of ASTM International*, vol. 8, no. 8, p. 103719, 2011.

[24] D. Chen, J. Zhou, and Q. Zhang, "Effects of heating rate on slow pyrolysis behavior, kinetic parameters and products properties of moso bamboo," *Bioresource Technology*, vol. 169, pp. 313–319, 2014.

[25] Y. Yao, B. Gao, M. Inyang et al., "Biochar derived from anaerobically digested sugar beet tailings: characterization and phosphate removal potential," *Bioresource Technology*, vol. 102, no. 10, pp. 6273–6278, 2011.

[26] X. Cao and W. Harris, "Properties of dairy-manure-derived biochar pertinent to its potential use in remediation," *Bioresource Technology*, vol. 101, no. 14, pp. 5222–5228, 2010.

[27] F. Ronsse, S. van Hecke, D. Dickinson, and W. Prins, "Production and characterization of slow pyrolysis biochar: influence of feedstock type and pyrolysis conditions," *GCB Bioenergy*, vol. 5, no. 2, pp. 104–115, 2013.

[28] Z. Wang, H. Guo, F. Shen et al., "Biochar produced from oak sawdust by Lanthanum (La)-involved pyrolysis for adsorption of ammonium (NH4+), nitrate (NO3-), and phosphate (PO43-)," *Chemosphere*, vol. 119, pp. 646–653, 2015.

[29] S. Kizito, S. Wu, W. Kipkemoi Kirui et al., "Evaluation of slow pyrolyzed wood and rice husks biochar for adsorption of ammonium nitrogen from piggery manure anaerobic digestate slurry," *Science of the Total Environment*, vol. 505, pp. 102–112, 2015.

[30] K. B. Cantrell, P. G. Hunt, M. Uchimiya, J. M. Novak, and K. S. Ro, "Impact of pyrolysis temperature and manure source on physicochemical characteristics of biochar," *Bioresource Technology*, vol. 107, pp. 419–428, 2012.

[31] Y. Sun, B. Gao, Y. Yao et al., "Effects of feedstock type, production method, and pyrolysis temperature on biochar and hydrochar properties," *Chemical Engineering Journal*, vol. 240, pp. 574–578, 2014.

[32] P. Devi and A. K. Saroha, "Simultaneous adsorption and dechlorination of pentachlorophenol from effluent by Ni-ZVI magnetic biochar composites synthesized from paper mill sludge," *Chemical Engineering Journal*, vol. 271, pp. 195–203, 2015.

[33] M. Stefaniuk and P. Oleszczuk, "Characterization of biochars produced from residues from biogas production," *Journal of Analytical and Applied Pyrolysis*, vol. 115, pp. 157–165, 2015.

[34] J. W. Gaskin, C. Steiner, K. Harris, K. C. Das, and B. Bibens, "Effect of low-temperature pyrolysis conditions on biochar for agricultural use," *Transactions of the ASABE*, vol. 51, no. 6, pp. 2061–2069, 2008.

[35] W. Wang, J. C. Martin, N. Zhang, C. Ma, A. Han, and L. Sun, "Harvesting silica nanoparticles from rice husks," *Journal of Nanoparticle Research*, vol. 13, no. 12, pp. 6981–6990, 2011.

[36] M. Ahmad, D. H. Moon, M. Vithanage et al., "Production and use of biochar from buffalo-weed (*Ambrosia trifida* L.) for trichloroethylene removal from water," *Journal of Chemical Technology and Biotechnology*, vol. 89, no. 1, pp. 150–157, 2014.

[37] T. J. Kinney, C. A. Masiello, B. Dugan et al., "Hydrologic properties of biochars produced at different temperatures," *Biomass & Bioenergy*, vol. 41, pp. 34–43, 2012.

[38] K. W. Jung, K. Kim, T. U. Jeong, and K. H. Ahn, "Influence of pyrolysis temperature on characteristics and phosphate adsorption capability of biochar derived from waste-marine macroalgae (Undaria pinnatifida roots)," *Bioresource Technology*, vol. 200, pp. 1024–1028, 2016.

[39] X. Xiao, B. Chen, and L. Zhu, "Transformation, morphology, and dissolution of silicon and carbon in rice straw-derived biochars under different pyrolytic temperatures," *Environmental Science & Technology*, vol. 48, no. 6, pp. 3411–3419, 2014.

[40] L. Qian and B. Chen, "Dual role of biochars as adsorbents for aluminum: The effects of oxygen-containing organic components and the scattering of silicate particles," *Environmental Science & Technology*, vol. 47, no. 15, pp. 8759–8768, 2013.

[41] H. Zheng, Z. Wang, X. Deng et al., "Characteristics and nutrient values of biochars produced from giant reed at different temperatures," *Bioresource Technology*, vol. 130, pp. 463–471, 2013.

[42] J. De Vrieze, A. M. Saunders, Y. He et al., "Ammonia and temperature determine potential clustering in the anaerobic digestion microbiome," *Water Research*, vol. 75, pp. 312–323, 2015.

[43] M. Inyang, B. Gao, Y. Yao et al., "Removal of heavy metals from aqueous solution by biochars derived from anaerobically digested biomass," *Bioresource Technology*, vol. 110, pp. 50–56, 2012.

[44] W. Zhang, S. Mao, H. Chen, L. Huang, and R. Qiu, "Pb(II) and Cr(VI) sorption by biochars pyrolyzed from the municipal wastewater sludge under different heating conditions," *Bioresource Technology*, vol. 147, pp. 545–552, 2013.

[45] S. A. Baig, J. Zhu, N. Muhammad, T. Sheng, and X. Xu, "Effect of synthesis methods on magnetic Kans grass biochar for enhanced As(III, V) adsorption from aqueous solutions," *Biomass & Bioenergy*, vol. 71, pp. 299–310, 2014.

[46] M. Kiliç, Ç. Kirbiyik, Ö. Çepelioğullar, and A. E. Pütün, "Adsorption of heavy metal ions from aqueous solutions by biochar, a by-product of pyrolysis," *Applied Surface Science*, vol. 283, pp. 856–862, 2013.

[47] Y. Xu and B. Chen, "Investigation of thermodynamic parameters in the pyrolysis conversion of biomass and manure to biochars using thermogravimetric analysis," *Bioresource Technology*, vol. 146, pp. 485–493, 2013.

[48] M. Waseem, S. Mustafa, A. Naeem, G. J. M. Koper, and Salah-Ud-Din, "Physiochemical properties of mixed oxides of iron and silicon," *Journal of Non-Crystalline Solids*, vol. 356, no. 50-51, pp. 2704–2708, 2010.

[49] Y. Xu and B. Chen, "Organic carbon and inorganic silicon speciation in rice-bran-derived biochars affect its capacity to adsorb cadmium in solution," *Journal of Soils and Sediments*, vol. 15, no. 1, pp. 60–70, 2014.

[50] P. Lu and Y. L. Hsieh, "Highly pure amorphous silica nano-disks from rice straw," *Powder Technology*, vol. 225, pp. 149–155, 2012.

[51] X. D. Cao, L. Q. Ma, M. Chen, S. P. Singh, and W. G. Harris, "Impacts of phosphate amendments on lead biogeochemistry at a contaminated site," *Environmental Science & Technology*, vol. 36, no. 24, pp. 5296–5304, 2002.

[52] X. Cao, L. Ma, B. Gao, and W. Harris, "Dairy-manure derived biochar effectively sorbs lead and atrazine," *Environmental Science & Technology*, vol. 43, no. 9, pp. 3285–3291, 2009.

[53] H. Lu, W. Zhang, Y. Yang, X. Huang, S. Wang, and R. Qiu, "Relative distribution of Pb^{2+} sorption mechanisms by sludge-derived biochar," *Water Research*, vol. 46, no. 3, pp. 854–862, 2012.


The Scientific
World Journal
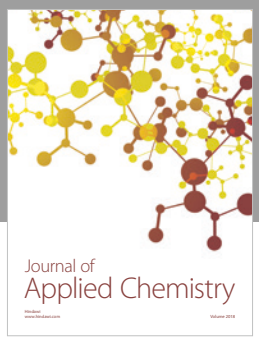
Journal of
Applied Chemistry
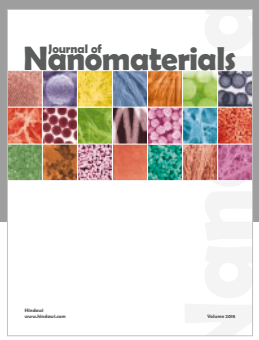
Journal of
Nanomaterials

Scientifica

International Journal of
Polymer Science
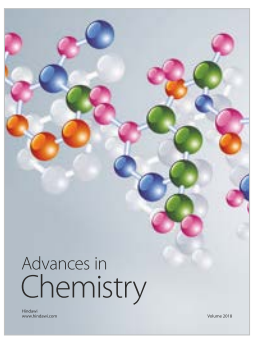
Advances in
Chemistry

Hindawi
Submit your manuscripts at
www.hindawi.com
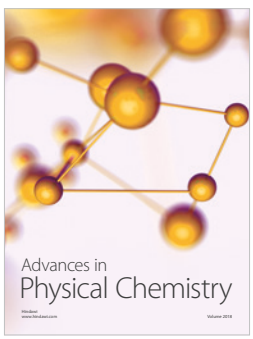
Advances in
Physical Chemistry

International Journal of
Analytical Chemistry
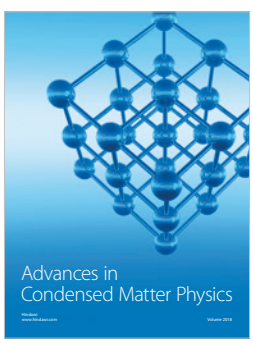
Advances in
Condensed Matter Physics
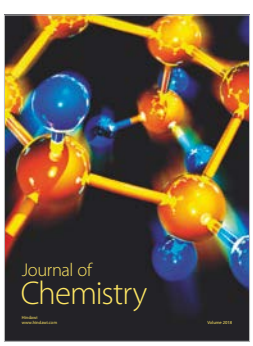
Journal of
Chemistry

International Journal of
Biomaterials
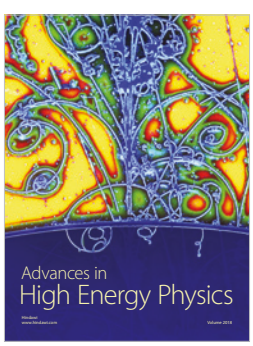
Advances in
High Energy Physics

Journal of
Engineering

Journal of
Nanotechnology

International Journal of
Corrosion

Journal of
Materials

BioMed
Research International
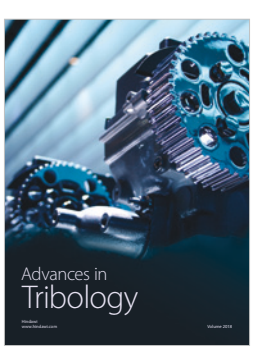
Advances in
Tribology
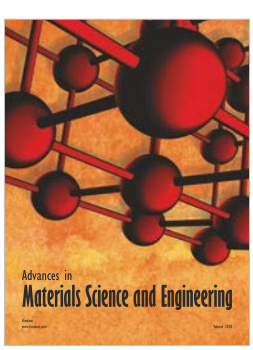
Advances in
Materials Science and Engineering